LETTER

doi:10.1038/nature21371

Reading and writing single-atom magnets

Fabian D. Natterer[1,2], Kai Yang[1,3], William Paul[1], Philip Willke[1,4], Taeyoung Choi[1], Thomas Greber[1,5], Andreas J. Heinrich[6,7] & Christopher P. Lutz[1]

The single-atom bit represents the ultimate limit of the classical approach to high-density magnetic storage media. So far, the smallest individually addressable bistable magnetic bits have consisted of 3–12 atoms[1–3]. Long magnetic relaxation times have been demonstrated for single lanthanide atoms in molecular magnets[4–12], for lanthanides diluted in bulk crystals[13], and recently for ensembles of holmium (Ho) atoms supported on magnesium oxide (MgO)[14]. These experiments suggest a path towards data storage at the atomic limit, but the way in which individual magnetic centres are accessed remains unclear. Here we demonstrate the reading and writing of the magnetism of individual Ho atoms on MgO, and show that they independently retain their magnetic information over many hours. We read the Ho states using tunnel magnetoresistance[15,16] and write the states with current pulses using a scanning tunnelling microscope. The magnetic origin of the long-lived states is confirmed by single-atom electron spin resonance[17] on a nearby iron sensor atom, which also shows that Ho has a large out-of-plane moment of 10.1 ± 0.1 Bohr magnetons on this surface. To demonstrate independent reading and writing, we built an atomic-scale structure with two Ho bits, to which we write the four possible states and which we read out both magnetoresistively and remotely by electron spin resonance. The high magnetic stability combined with electrical reading and writing shows that single-atom magnetic memory is indeed possible.

The demonstration of magnetic bistability in single-molecule magnets containing one rare-earth atom[4,6,9,11] illustrated the potential of single-atom spin centres in future storage media[5,7,8,10,12]. A ligand field that provides a barrier against magnetization reversal by lifting the Hund degeneracies in single-molecule magnets[4–11] can also be realized for atoms bound to a surface[18–21]. While a break junction probes the quantum states of one isolated molecule[22], a surface enables preparation of and access to numerous spin centres. Magnetic lifetimes in the range of milliseconds were accordingly obtained for single 3*d* atoms on MgO (ref. 23), but a recent report of magnetic bistability for Ho atoms on a platinum surface is debated[3,24–26]. A major advance of observing magnetic remanence was recently achieved with an ensemble of isolated Ho atoms on MgO (ref. 14), yet the question remained whether electrical probing of the highly localized *f* orbitals of individual rare-earth atoms is possible[3,27,28].

Here we address the magnetic bistability of individual Ho atoms on MgO, which we switch using current pulses and detect through the tunnel magnetoresistance using a spin-polarized scanning tunnelling microscope (STM)[15]. We unambiguously prove the magnetic origin of the switching in the tunnelling resistance using STM-enabled single-atom electron spin resonance (ESR) on an adjacent iron (Fe) sensor atom. Additionally, we determine by this method the out-of-plane component of the Ho magnetic moment, and use the long lifetime to store two bits of information in an array of two Ho atoms

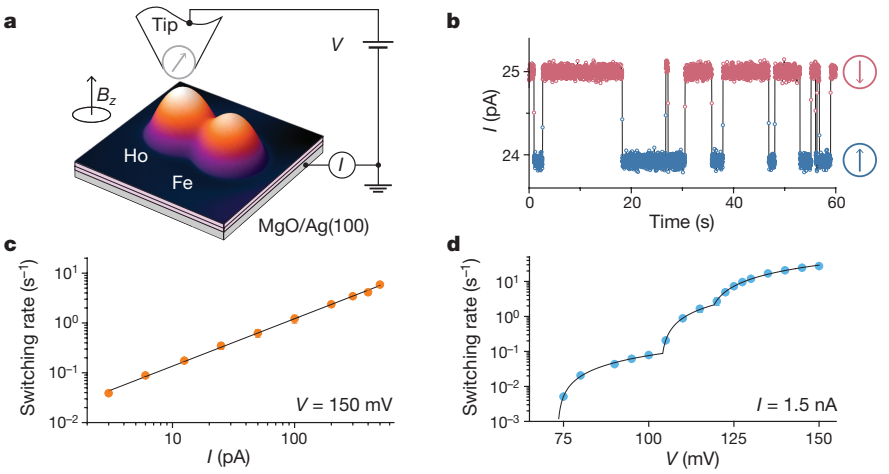

Figure 1 | Experimental set-up and magnetic switching of holmium. **a**, Topographic image of a Ho and an Fe atom on bilayer MgO. The magnetic states of Ho are controlled and probed with an STM using spin-polarized tunnelling ($V = 10$ mV, $I = 10$ pA, 2.35 nm × 2.35 nm, $T = 1.2$ K, $B_z \approx 100$ mT). **b**, The magnetoresistive tunnel current I recorded atop a Ho atom (STM image in **a**) shows switching between two magnetic states (red, down; blue, up) of long residence time ($V = 150$ mV, current set point $I = 25$ pA). At these tunnelling conditions, switching is induced by tunnelling electrons. **c**, The switching rate Γ at $B_z \approx 50$ mT scales as $\Gamma = a(I/I_0)^N$, where N is close to unity and a is a switching coefficient (see Methods, $V = 150$ mV, $I_0 = 1$ pA). **d**, The voltage dependence at $B_z \approx 50$ mT of Γ at constant current ($I = 1.5$ nA) reveals three rate-increasing thresholds at $V_1 = 73 \pm 1$ mV, $V_2 = 104 \pm 1$ mV and $V_3 = 119 \pm 1$ mV. The solid line is a three-segment piecewise linear fit. The uncertainty of the fits in **c** and **d** indicate the standard deviation on the least-squares fit parameter.

[1]IBM Almaden Research Center, San Jose, California 95120, USA. [2]Institute of Physics, École Polytechnique Fédérale de Lausanne, CH-1015 Lausanne, Switzerland. [3]School of Physical Sciences and Key Laboratory of Vacuum Physics, University of Chinese Academy of Sciences, Beijing 100049, China. [4]IV. Physical Institute, University of Göttingen, Friedrich-Hund-Platz 1, D-37077 Göttingen, Germany. [5]Physik-Institut, Universität Zürich, Winterthurerstrasse 190, CH-8057 Zürich, Switzerland. [6]Institute of Basic Science, Center for Quantum Nanoscience, Seoul, South Korea. [7]Physics Department, Ewha Womans University, Seoul, South Korea.

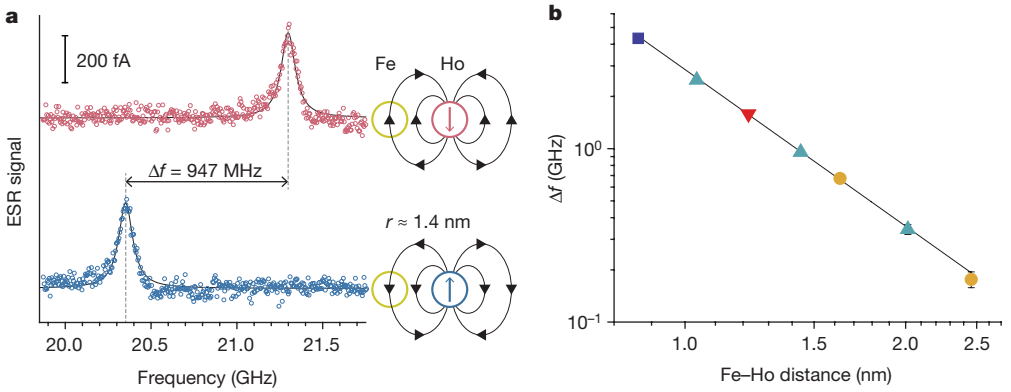

Figure 2 | Controlling and measuring the magnetic states of holmium. **a**, Electron spin resonance (ESR) spectrum of an Fe sensor for Ho in the high-conductance (top, red) and low-conductance (bottom, blue) state. The continuous black lines are fits to a single Lorentzian and were used to extract the resonance frequencies of the ESR signal ($V = 60$ mV, $I = 20$ pA, $V_{RF} = 15$ mV zero-to-peak, $B_z \approx 100$ mT). The inset schematics show the dipolar field of the Ho atom in the up and down states. **b**, A log–log plot of the frequency difference Δf for different Fe–Ho distances (data points) shows excellent agreement with a magnetic dipole–dipole interaction (line) and follows a power law with a power index (slope in the log–log plot) of -3. The one-parameter fit yields a Ho magnetic moment of $(10.1 \pm 0.1)\mu_B$. The uncertainty accounts for the standard error on the least-squares fit parameter and the error propagation from the magnetic moment of the Fe sensor. Measurements of different Ho atoms (coded with distinct symbols) show identical moments.

whose magnetic state can be read locally by magnetoresistance, and remotely by means of ESR on a nearby sensor atom.

Figure 1 shows our experimental set-up consisting of a low-temperature STM with ESR capability[17], which uses an Fe atom as a local magnetometer to determine nearby magnetic moments[29]. A total magnetic field $B = 0.495$–0.9 T is applied nearly in-plane, yielding an out-of-plane component $B_z \approx 50$–100 mT that sets the Zeeman splitting of the Fe field sensor[17]. Upon dosing Ho on bilayer MgO, we find individually adsorbed Ho atoms in two binding sites: atop oxygen and on bridge sites, in agreement with previous reports[14]. Here we focus on Ho atoms atop oxygen—the Ho species that shows long lifetime[14]—and note that we can move individual Ho atoms from bridge to oxygen sites by using the STM tip and by applying voltage pulses. The co-adsorbed Fe sensor atoms can be distinguished from Ho by a lower topographic height and by their spectroscopic fingerprint: Fe atoms show inelastic spin excitations at approximately 14 meV (ref. 21); Ho atoms are devoid of spin-excitation signatures. However, we measure a two-state signal on Ho atoms that shows discrete changes in conductance of typically 2%–4% with a spin-polarized tip (Fig. 1b). The current trace has plateaus of long residence times in the high- and low-conductance states. For the sample bias voltage $V = 150$ mV used in Fig. 1c, the magnetic residence time ranges from dozens of seconds to fractions of a second for tunnel currents $I = 6$–600 pA. The essentially linear increase in the switching rate (Methods) with tunnel current indicates a single-electron rate-limiting process with a miniscule switching probability of the order of 10^{-9} per tunnelling electron (see also Extended Data Fig. 1). We observe that the Ho states remain stable for hours when the bias voltage is kept below $|V| \approx 73$ mV (Extended Data Fig. 1). At higher voltages we see an increasing switching rate of the Ho states with bias voltage (Fig. 1d). We therefore have two means to control the switching rate: the tunnel current and the bias voltage. To write the Ho state, we repeatedly subject the Ho atom to a current pulse at $V > 150$ mV, until we detect a change in magnetoresistance at $V = 50$ mV that indicates that the Ho atom is in the desired final state. Three rate-increasing voltage thresholds appear in Fig. 1d and Extended Data Fig. 1, which may reflect transition energies between different magnetic states of Ho on MgO.

In the following, we use a nearby Fe sensor atom to prove that the two Ho states correspond to two magnetic orientations of the Ho moment. The Fe sensor acts as a local magnetometer[29] because the Zeeman splitting of its ground states responds to the dipolar field of the nearby Ho atom. The Zeeman splitting of the Fe sensor, which is dominated by the external out-of-plane magnetic field B_z, is therefore shifted to lower frequency when the Ho moment is aligned in the direction of B_z, and to higher frequency when it is aligned in the direction of $-B_z$. The ESR spectrum on the Fe sensor in Fig. 2a revealed a single resonance peak when Ho was in its high-conductance state. After switching Ho to the low-conductance state, the ESR peak correspondingly shifted to lower frequency. We find that the frequency difference Δf sensitively depends on the Fe–Ho distance, as seen in Fig. 2b. The identical scaling for different Fe–Ho pairs shows the equivalent magnetic structure among distinct Ho atoms. Following previous work[29], we describe the Δf versus distance scaling in terms of the magnetic dipole–dipole interaction for out-of-plane polarized moments. Using the Fe moment of $(5.44 \pm 0.03)\mu_B$ (where μ_B is the Bohr magneton and the error given here and elsewhere represents the standard deviation in the fit parameter) on the same MgO/Ag(100) surface[29], a one-parameter fit yields the Ho moment of $(10.1 \pm 0.1)\mu_B$. A magnetic moment of 10.1 μ_B suggests a $4f^{10}$ Ho(III) ion configuration where its total angular momentum J is polarized out-of-plane ($J_z = \pm 8$). Note that we are sensing the out-of-plane component of the total magnetic moment, which includes contributions from all orbitals in addition to the dominant $4f$ electrons (see Methods). The previously deduced lower J_z value[14] could be influenced by the averaging over Ho atoms in different adsorption sites on MgO in the X-ray ensemble measurements (see Methods).

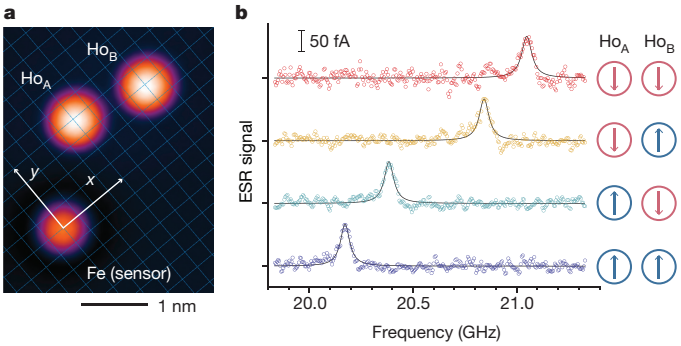

Figure 3 | Example of a stable two-bit atomic Ho array. **a**, The Ho atoms (Ho_A and Ho_B) were arranged in an $(x, y) = (4, 4)$ and an $(x, y) = (8, 3)$ configuration with respect to the Fe sensor, measured in increments of the oxygen sublattice ($V = 60$ mV, $I = 6$ pA). **b**, ESR spectra demonstrating simultaneous read-out as measured on the Fe sensor atom ($V = 60$ mV, $I = 20$ pA, $V_{RF} = 15$ mV, $B_z \approx 100$ mT). All four states can be read out in a single ESR spectrum. The only change in the magnetic states occurred after deliberately switching the Ho atoms and no spontaneous reversal was observed over several hours. The black solid lines are fits to Lorentzian curves.

Most importantly, however, the correlation of Ho in high- and low-conductance states to the respective ESR frequencies unambiguously proves the magnetic origin of the two-state switching for Ho. In addition, the presence of only one ESR peak in each spectrum acquired over many minutes is a consequence of the extraordinary stability of the magnetic state of the Ho atom.

The high stability of the Ho moment could find use in single-atom data storage applications. To exemplify this point, we built a stable two-bit atomic Ho array (Fig. 3a) and measured the Ho states non-invasively using ESR on a nearby Fe sensor (Fig. 3b). The frequency differences between the four ESR lines were engineered with the knowledge of our dipole–dipole data in Fig. 2b in mind. Accordingly, after setting the Ho bits individually to their up and down states, we observe one of four distinct ESR lines on the Fe sensor, identifying the four possible states of the Ho bit array. During the 5 h of deliberately reading and writing the magnetic states of the atoms at 1.2 K, we did not observe unintended magnetic switching of the neighbouring atom. Similarly, monitoring the ESR frequency at 4.3 K confirmed the stability of the Ho states at higher temperature (Extended Data Fig. 2).

The use of single-atom magnets as building blocks in complex structures should enable future studies of magnetic interactions ranging from pairwise coupling to collective behaviour emerging from dense magnetic arrays, such as in geometrically frustrated systems[30].

Online Content Methods, along with any additional Extended Data display items and Source Data, are available in the online version of the paper; references unique to these sections appear only in the online paper.

Received 20 August 2016; accepted 9 January 2017.

1. Loth, S., Baumann, S., Lutz, C. P., Eigler, D. M. & Heinrich, A. J. Bistability in atomic-scale antiferromagnets. *Science* **335,** 196–199 (2012).
2. Khajetoorians, A. A. *et al.* Current-driven spin dynamics of artificially constructed quantum magnets. *Science* **339,** 55–59 (2013).
3. Steinbrecher, M. *et al.* Absence of a spin-signature from a single Ho adatom as probed by spin-sensitive tunneling. *Nat. Commun.* **7,** 10454 (2016).
4. Ishikawa, N., Sugita, M., Ishikawa, T., Koshihara, S.-Y. & Kaizu, Y. Lanthanide double-decker complexes functioning as magnets at the single-molecular level. *J. Am. Chem. Soc.* **125,** 8694–8695 (2003).
5. Bogani, L. & Wernsdorfer, W. Molecular spintronics using single-molecule magnets. *Nat. Mater.* **7,** 179–186 (2008).
6. Kyatskaya, S. *et al.* Anchoring of rare-earth-based single-molecule magnets on single-walled carbon nanotubes. *J. Am. Chem. Soc.* **131,** 15143–15151 (2009).
7. Rinehart, J. D. & Long, J. R. Exploiting single-ion anisotropy in the design of f-element single-molecule magnets. *Chem. Sci.* **2,** 2078–2085 (2011).
8. Gatteschi, D., Sessoli, R. & Villain, J. *Molecular Nanomagnets* (Oxford Univ. Press, 2011).
9. Westerström, R. *et al.* An endohedral single-molecule magnet with long relaxation times: $DySc_2N@C_{80}$. *J. Am. Chem. Soc.* **134,** 9840–9843 (2012).
10. Liddle, S. T. & van Slageren, J. Improving f-element single molecule magnets. *Chem. Soc. Rev.* **44,** 6655–6669 (2015).
11. Wäckerlin, C. *et al.* Giant hysteresis of single-molecule magnets adsorbed on a nonmagnetic insulator. *Adv. Mater.* **28,** 5195–5199 (2016).
12. Layfield, R. A. Organometallic single-molecule magnets. *Organometallics* **33,** 1084–1099 (2014).
13. Giraud, R., Wernsdorfer, W., Tkachuk, A. M., Mailly, D. & Barbara, B. Nuclear spin driven quantum relaxation in $LiY_{0.998}Ho_{0.002}F_4$. *Phys. Rev. Lett.* **87,** 057203 (2001).
14. Donati, F. *et al.* Magnetic remanence in single atoms. *Science* **352,** 318–321 (2016).
15. Wiesendanger, R. Spin mapping at the nanoscale and atomic scale. *Rev. Mod. Phys.* **81,** 1495–1550 (2009).
16. Loth, S., Lutz, C. P. & Heinrich, A. J. Spin-polarized spin excitation spectroscopy. *New J. Phys.* **12,** 125021 (2010).
17. Baumann, S. *et al.* Electron paramagnetic resonance of individual atoms on a surface. *Science* **350,** 417–420 (2015).
18. Gambardella, P. *et al.* Giant magnetic anisotropy of single cobalt atoms and nanoparticles. *Science* **300,** 1130–1133 (2003).
19. Khajetoorians, A. A. *et al.* Spin excitations of individual Fe atoms on Pt(111): impact of the site-dependent giant substrate polarization. *Phys. Rev. Lett.* **111,** 157204 (2013).
20. Donati, F. *et al.* Tailoring the magnetism of Co atoms on graphene through substrate hybridization. *Phys. Rev. Lett.* **113,** 177201 (2014).
21. Baumann, S. *et al.* Origin of perpendicular magnetic anisotropy and large orbital moment in Fe atoms on MgO. *Phys. Rev. Lett.* **115,** 237202 (2015).
22. Vincent, R., Klyatskaya, S., Ruben, M., Wernsdorfer, W. & Balestro, F. Electronic read-out of a single nuclear spin using a molecular spin transistor. *Nature* **488,** 357–360 (2012).
23. Paul, W. *et al.* Control of the millisecond spin lifetime of an electrically probed atom. *Nat. Phys.* http://dx.doi.org/10.1038/NPHYS3965 (2016).
24. Miyamachi, T. *et al.* Stabilizing the magnetic moment of single holmium atoms by symmetry. *Nature* **503,** 242–246 (2013).
25. Donati, F. *et al.* Magnetism of Ho and Er atoms on close-packed metal surfaces. *Phys. Rev. Lett.* **113,** 237201 (2014).
26. Khajetoorians, A. A. & Heinrich, A. J. Toward single-atom memory. *Science* **352,** 296–297 (2016).
27. Coffey, D. *et al.* Antiferromagnetic spin coupling between rare earth adatoms and iron islands probed by spin-polarized tunneling. *Sci. Rep.* **5,** 13709 (2015).
28. Meservey, R., Paraskevopoulos, D. & Tedrow, P. M. Tunneling measurements of conduction-electron-spin polarization in heavy rare-earth metals. *Phys. Rev. B* **22,** 1331–1337 (1980).
29. Choi, T. *et al.* Atomic-scale sensing of the magnetic dipolar field from single atoms. *Nat. Nanotechnol.* http://dx.doi.org/10.1038/nnano.2017.18 (2017).
30. Lacroix, C., Mendels, P. & Mila, F. *Introduction to Frustrated Magnetism: Materials, Experiments, Theory* (Springer, 2011).

Acknowledgements We thank B. Melior for technical assistance and F. Donati for discussions. We acknowledge financial support from the Office of Naval Research. F.D.N. appreciates support from the Swiss National Science Foundation under project numbers P300P2_158468 and PZ00P2_167965, and help from A. Natterer. K.Y. acknowledges support from National Natural Science Foundation of China (grant number 61471337). W.P. thanks the Natural Sciences and Engineering Research Council of Canada for fellowship support. P.W. acknowledges financial support from the German academic exchange service. T.G. thanks B. Delley for discussions and IBM Research for its hospitality.

Author Contributions F.D.N. conceived the experiment and wrote the manuscript. F.D.N., K.Y., W.P. and P.W. analysed the data. W.P. conceived the atom-switching routine. C.P.L. and A.J.H. enabled and supervised the project. All authors carried out measurements, discussed the results and contributed to the manuscript.

Author Information Reprints and permissions information is available at www.nature.com/reprints. The authors declare no competing financial interests. Readers are welcome to comment on the online version of the paper. Correspondence and requests for materials should be addressed to F.D.N. (fabian.natterer@epfl.ch), A.J.H. (heinrich@ewha.ac.kr) and C.P.L. (cplutz@us.ibm.com).

Reviewer Information *Nature* thanks N. Lorente, R. Sessoli and W. Wernsdorfer for their contribution to the peer review of this work.

METHODS

Experimental methods. We performed the experiments in a custom-built Joule–Thomson low-temperature STM, working in ultrahigh vacuum at 1.2 K, and carried out ESR measurements by adding a radio-frequency voltage of typically $V_{RF} = 15$ mV zero-to-peak at 10–30 GHz onto the DC bias voltage[17,31]. A total magnetic field of 0.9 T was applied mostly in-plane with a B_z component of about 100 mT providing a Zeeman splitting of about 20.8 GHz for our Fe sensors. We dosed Ho and Fe atoms from pieces of pure metal with e-beam evaporators directly onto the sample held at a temperature below 10 K. The STM tip was an Ir wire that had been conditioned by field emission and subsequent indentations into the Ag crystal until it became coated by Ag and atomically sharp. We spin-polarized our tips by picking up Fe atoms (typically one to five) until pump-probe measurements on Fe sensors yielded spin contrast. To grow MgO, we exposed an atomically clean Ag(100) single crystal, held at about 600 K, to an Mg flux from a Knudsen cell in an oxygen partial pressure of about 10^{-6} mbar up to a MgO coverage of 1.5 monolayers. The growth rate was about 0.5 monolayers per minute (refs 32, 33). We assumed in-plane commensurability between the Ag and MgO lattices and a low-temperature Ag lattice parameter of 406.87 pm (ref. 29). All atoms were studied on bilayer MgO as determined by the conductance at point contact[23]. This bilayer thickness had previously been denoted as monolayer MgO (ref. 17).

Ho switching-rate analysis. The Ho switching rate was measured for negative and positive bias voltages at a total field $B = 0.495$ T and current of 1.5 nA (Extended Data Fig. 1a). We find the same three rate-increasing voltage thresholds presented in Fig. 1d for negative polarity. From a piecewise linear fit of the form $\Gamma = \sum_{i=1}^{3} c_i(V - V_i)/V_i$ between ±70 mV and ±150 mV, we obtain the threshold values and coefficients displayed in Extended Data Fig. 1c. The Ho switching rate shown in Fig. 1c, d and Extended Data Fig. 1 accounts for the total number of switches—from the up to the down state and vice versa. Because the switching rate becomes too rapid at higher bias values, we obtain a further measure of the fast switching rate by reduced-duty-cycle switching, following the method described ref. 1. With this technique, we subject the atom to a low-duty-cycle train of high-voltage pulses (0.1 ms pulse every 0.5 ms) and probe whether the atom has reversed its magnetization using a sub-switching-threshold voltage for read-out. For all switching measurements, the field is applied mostly in-plane with an out-of-plane component of $B_z \approx 50$ mT at a total field of 0.495 T. No further voltage thresholds appear up to the maximum voltages probed, ±300 mV, and the switching rate effectively levelled off to approach a constant probability of switching of about 10^{-8} per tunnelling electron, independent of the voltage. This suggests that the tunnelling electrons assist reversal of the magnetic state primarily via the 119-mV transition.

The tunnelling-current-dependent switching rate was measured at different magnetic fields and bias voltages (Extended Data Fig. 1b). The switching rate follows a power law, $\Gamma = a(I/I_0)^N$, in all cases, with an exponent N close to unity, similar to what is shown in Fig. 1c. The fit parameters are: $a = (3 \pm 0.3) \times 10^{-3}\,s^{-1}$ and $N = 0.8 \pm 0.1$ at 120 mV and 0.9 T; $a = (4 \pm 2) \times 10^{-2}\,s^{-1}$ and $N = 0.9 \pm 0.1$ at 150 mV and 0.9 T; and $a = (1.5 \pm 0.1) \times 10^{-2}\,s^{-1}$ and $N = 0.95 \pm 0.01$ at 150 mV and 0.495 T. The uncertainties represent the standard deviation in the fit parameter. The switching rates at 0.495 T ($B_z \approx 50$ mT) and 0.9 T ($B_z \approx 100$ mT) are comparable, but slightly higher at the larger field. A polynomial background was subtracted from the current trace in Fig. 1b to correct for a tip drift of approximately 10 pm. We did not measure switching rates at even smaller fields because a certain magnetic field is required to magnetically polarize the tip, which we need to obtain spin-polarized tunnel currents.

Thermal stability. We monitored the stability of the Ho moment at 4.3 K and 0.9 T for several hours using ESR on a nearby Fe sensor atom (Extended Data Fig. 2). We first determined the frequency of the ESR lines for Ho in the up and down states. In the case shown in Extended Data Fig. 2, the separation between the Ho atom and the Fe sensor was approximately 1.4 nm and, correspondingly, a frequency difference of about 1 GHz was found. We then tracked the ESR intensity at the two frequencies (Extended Data Fig. 2b). After 1.55 h, we observed one reversal of ESR intensities (the ESR peak moved from the spin-down to the spin-up frequency in Extended Data Fig. 1b), which corresponds to a switch of the Ho moment. The Ho moment stayed in that new state for the remainder of the inspection (about 2 h). This single spontaneous reversal event could be due to either the increased temperature or hot electrons that made it from the STM tip to the Ho atom. During that measurement the STM tip was positioned above the Fe sensor, which was placed a few lattice sites away. A radio-frequency voltage of 25 mV (zero-to-peak) was added to the 60-mV DC bias, which yielded a peak voltage of 85 mV. It is therefore a possibility that the reversal was induced by stray tunnelling electrons having a larger energy than the switching threshold of 73 mV (Fig. 1d and Extended Data Fig. 1a). In any case, the data exemplifies the extraordinary stability of the Ho moment on MgO at 4.3 K. We were not able to further increase the measurement temperature, owing to limitations of the apparatus, including a reduced spin-polarization of the STM tips at elevated temperatures. The X-ray experiments[14] independently demonstrate stability to temperatures exceeding 30 K.

Difference of the Ho moment with respect to X-ray results. An apparent discrepancy between the value for the out-of-plane Ho moment measured by ESR (10.1 μ_B) here and the value deduced from X-ray absorption spectroscopy (approximately 5.7 μ_B)[14] is evident. One possible origin of this discrepancy can be found by questioning what aspect of the Ho atom is measured by ESR. Here, the out-of-plane component of the total magnetic field created by the Ho atom at the location of the Fe sensor atom is measured. Although this field certainly arises primarily from the 4*f* electrons, it contains the contributions from all other open orbitals as well. In addition, the spatial averaging over a distribution of spin centres in various binding sites might influence the outcome of the X-ray method. For Ho/MgO, this could be the presence of a fraction of Ho atoms residing in a bridge site instead of solely on the oxygen site. In fact, previous STM data shows an MgO-thickness-dependent preference for Ho in a bridge (0–2 monolayers) or oxygen site (>3 monolayers)[14]. The same STM measurements also show a quasi-layer-by-layer growth of MgO, that is, surface terminations of different thicknesses and of distinct adsorption site preference for each of these thicknesses. The X-ray beam spot would accordingly average over both Ho atom species, leading to a different effective magnetic moment.

Data availability. The main data that support the findings of this study are available within the paper (including its Methods and Extended Data); Source Data for Figs 1c, d and 2b, and Extended Data Fig. 1a, b are available in the online version of the paper. Additional data are available from F.D.N. (fabian.natterer@epfl.ch) on reasonable request.

31. Paul, W., Baumann, S., Lutz, C. P. & Heinrich, A. J. Generation of constant-amplitude radio-frequency sweeps at a tunnel junction for spin resonance STM. *Rev. Sci. Instrum.* **87,** 074703 (2016).
32. Schintke, S. & Schneider, W.-D. Insulators at the ultrathin limit: electronic structure studied by scanning tunnelling microscopy and scanning tunnelling spectroscopy. *J. Phys. Condens. Matter* **16,** R49–R81 (2004).
33. Pal, J. *et al.* Morphology of monolayer MgO films on Ag(100): switching from corrugated islands to extended flat terraces. *Phys. Rev. Lett.* **112,** 126102 (2014)

a

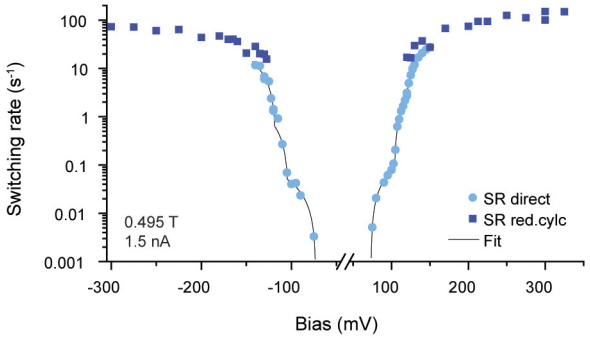

b

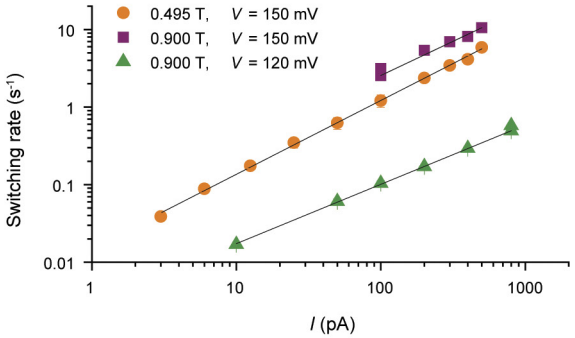

c

	-V	+V
V_1 (mV)	-73.0 ± 1.3	73.0 ± 0.1
V_2 (mV)	-104.6 ± 0.3	104.1 ± 0.1
V_3 (mV)	-118.6 ± 0.6	119.2 ± 0.3
c_1 (s^{-1})	0.12 ± 0.02	0.21 ± 0.01
c_2 (s^{-1})	4.2 ± 0.5	13.9 ± 0.6
c_3 (s^{-1})	58 ± 7	89 ± 3

Extended Data Figure 1 | Switching-rate dependence of Ho atoms on MgO/Ag(100). a, Switching rate at a constant current of 1.5 nA and a total field of 0.495 T ($B_z \approx 50$ mT). The three threshold values (listed in **c**) are identical for positive and negative bias. The light blue circles represent the switching rate that was directly measured from current traces and the dark blue squares show a reduced-duty-cycle measurement for higher switching rates. The black line stems from a piecewise linear fit. **b**, The current-dependent switching rates follow a power law that has an exponent close to unity for all field and bias conditions. This scaling behaviour indicates a single-electron rate-limiting process in the reversal of the Ho moment by energetic electrons. **c**, Fit parameters for the switching rate in **a**. The uncertainties represent the standard deviation in the fit value.

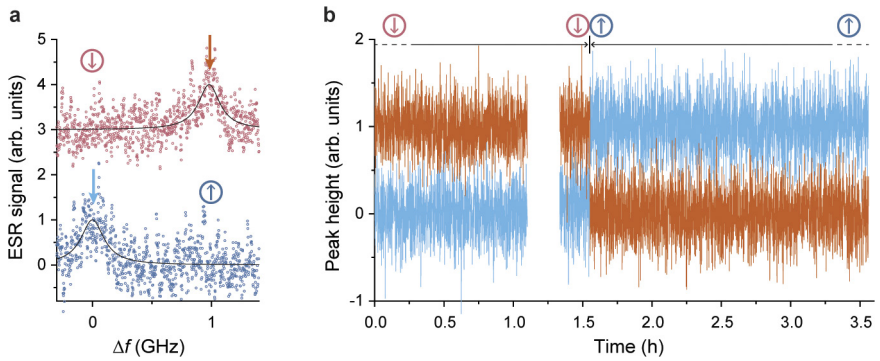

Extended Data Figure 2 | Temporal stability of a Ho bit at 4.3 K measured with STM-ESR. a, ESR spectra for up (top, red) and down (bottom, blue) alignment of the Ho bit at 4.3 K. The sweeps were normalized to the ESR peak height and vertically offset for clarity. **b**, Monitoring the ESR signal at the two frequencies corresponding to up (blue) and down (orange) alignment of the Ho bit (arrows in **a**) versus time t ($V = 60$ mV, $I = 20$ pA, $V_{RF} = 25$ mV). The Ho bit spontaneously switches to the up state at $t = 1.55$ h and remains in that state for the remainder of the sweep. A polynomial background was subtracted from each trace to correct for lateral tip drift. The gap at $t = 1.1$ h is an interruption that was used to realign the tip onto the Fe sensor to correct for tip drift.